ACS APPLIED MATERIALS & INTERFACES

Research Article

Cite This: ACS Appl. Mater. Interfaces 2019, 11, 17863−17872

www.acsami.org

Understanding the Static Interfacial Polymer Layer by Exploring the Dispersion States of Nanocomposites

Anne-Caroline Genix,*[,†,‡] Vera Bocharova,*[,†] Bobby Carroll,[¶] Michelle Lehmann,[†,▽] Tomonori Saito,[†,▽] Susan Krueger,[§] Lilin He,[∥] Philippe Dieudonné-George,[‡] Alexei P. Sokolov,[†,⊥] and Julian Oberdisse[‡]

[†]Chemical Sciences Division, Oak Ridge National Laboratory, Oak Ridge, Tennessee 37831, United States

[‡]Laboratoire Charles Coulomb (L2C), Université de Montpellier, CNRS, F-34095 Montpellier, France

[§]NIST Center for Neutron Research, NIST, Gaithersburg, Maryland 20899, United States

[∥]Neutron Scattering Division, Oak Ridge National Laboratory, Oak Ridge, Tennessee 37831, United States

[⊥]Department of Chemistry, University of Tennessee, Knoxville, Tennessee 37996, United States

[¶]Department of Physics and Astronomy, University of Tennessee, Knoxville, Tennessee 37996, United States

[▽]The Bredesen Center for Interdisciplinary Research and Graduate Education, University of Tennessee, Knoxville, Tennessee 37996, United States

Supporting Information

ABSTRACT: The dynamic and static properties of the interfacial region between polymer and nanoparticles have wide-ranging consequences on performances of nanomaterials. The thickness and density of the static layer are particularly difficult to assess experimentally due to superimposing nanoparticle interactions. Here, we tune the dispersion of silica nanoparticles in nanocomposites by preadsorption of polymer layers in the precursor solutions, and by varying the molecular weight of the matrix chains. Nanocomposite structures ranging from ideal dispersion to repulsive order or various degrees of aggregation are generated and observed by small-angle scattering. Preadsorbed chains are found to promote ideal dispersion, before desorption in the late stages of nanocomposite formation. The microstructure of the interfacial polymer layer is characterized by detailed modeling of X-ray and neutron scattering. Only in ideally well-dispersed systems a static interfacial layer of reduced polymer density over a thickness of ca. 2 nm is evidenced based on the analysis with a form-free density profile optimized using numerical simulations. This interfacial gradient layer is found to be independent of the thickness of the initially adsorbed polymer, but appears to be generated by out-of-equilibrium packing and folding of the preadsorbed layer. The impact of annealing is investigated to study the approach of equilibrium, showing that initially ideally well-dispersed systems adopt a repulsive hard-sphere structure, while the static interfacial layer disappears. This study thus promotes the fundamental understanding of the interplay between effects which are decisive for macroscopic material properties: polymer-mediated interparticle interactions, and particle interfacial effects on the surrounding polymer.

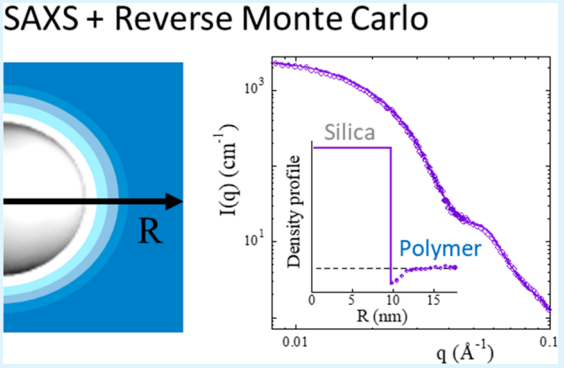

KEYWORDS: *polymer nanocomposites, interfacial layer, density gradient, nanoparticle dispersion, chain adsorption, small-angle scattering, reverse Monte Carlo*

1. INTRODUCTION

The dispersion of nanoparticles (NPs) and their interactions in polymer matrices are key factors influencing thermal[1] and mechanical properties of polymer nanocomposites (PNCs).[2,3] In particular, contact between NPs within aggregates or percolating networks provides transmission paths of forces,[4,5] or electric charges.[6] On the other end of the spectrum, individual dispersion allows taking advantage of the high specific surface of NPs. The optimum choice for material performance depends on the rubbery or glassy state of the polymer matrix: in the melt state, e.g., NP aggregation contributes to the improvement of mechanical properties,[7] whereas well-dispersed NPs are required for their optimization below the glass-transition temperature.[8] Moreover, the modification of static[9,10] or dynamical[11,12] properties in the interfacial region may strongly impact macroscopic properties, both through its influence on effective NP interactions, and through NP−polymer interactions governing the rheological

Received: March 13, 2019
Accepted: April 22, 2019
Published: April 22, 2019

DOI: 10.1021/acsami.9b04553
ACS Appl. Mater. Interfaces 2019, 11, 17863−17872

and thermodynamic properties of the interface itself. It is thus crucial to have detailed information (density, glass transition, ...) on the interfacial regions, which have well-established dynamical signatures,[12] but only a scarcely known static structure. This is mainly due to the relevance of highly concentrated systems for polymer nanocomposites. Measurements by small-angle X-ray scattering (SAXS) have been attempted to characterize density in the interfacial layer,[13,14] but the presence of strong and unknown interactions between highly polydisperse particles makes it difficult to attribute scattering features unambiguously to the density of a thin and weakly contributing surface layer, which moreover may be affected by nonequilibrium effects. It is the purpose of the present article to measure the static structure of interfacial layers by fine-tuning dispersion properties.

The thermodynamics of the mixing process of NPs with any matrix results from a sum of NP−NP and NP−polymer interactions:[15−17] In many experimental systems, NPs tend to demix spontaneously due to the hydrophilicity of their surface, which is opposed to the hydrophobicity of most polymers. Long-range interactions, in particular electrostatic ones, may prevent NP contact and thus aggregation if the PNCs are obtained by solvent casting.[18] Surface modification of NPs has been studied extensively, either with small surfactant-like molecules,[19] or polymer chain grafting.[20,21] In both cases, the NPs are compatibilized with the matrix, and a steric repulsion layer prevents interparticle contact and NP agglomeration, for example by depletion interaction during film formation. The polymer may be adsorbed (physisorbed) in case of an attraction with the NP, like e.g., hydrogen bonding between the polymer and hydroxyl groups of silica NPs.[22] The absence of covalent bonds provides an additional degree of freedom, as chains can then move. If the chains have sufficient mobility, for instance at high temperature, they can maximize global entropy by mixing with the matrix polymer. The system free energy, however, will in general be minimized by a partition with a portion of the chains sticking to the surface for enthalpic reasons. Finally, colloidal interactions are not the only factors: external and possibly out-of-equilibrium processes driven by annealing[23−25] or mixing (casting, precipitation[26] or solid-state mixing[27]) may strongly influence the final dispersion. The resulting driving forces may modify the balance between competing processes, like the speed of drying vs the viscosity and thus the time-scale of collision of NPs in the precursor solution.[28] Structural rearrangement of NPs during drying has been followed in situ using SAXS.[18,29] The many ways to modify NP interactions summarized here suggests that a library of formulations can be used to tailor dispersions, and we will take advantage of this library in the present paper.

In PNCs with attractive interactions, an adsorbed polymer layer (also called a bound layer)[30] forms naturally on the NP surface, with an average thickness in the dry state determined by thermogravimetric analysis (TGA)[31,32] of the order of the polymer radius of gyration, R_g.[33,34] The latter can be measured by isotopic labeling and small-angle neutron scattering (SANS).[35] The bound layer is expected to be somewhat thicker than estimated using the bulk density due to swelling, inducing long-range interactions between NPs, as confirmed by dynamic light scattering in solution, or in PNCs based on effective interparticle interactions.[34] Additionally, these adsorbed chains lead to a dynamic interfacial layer (DIL) extending typically over 2−6 nm around the NPs, which displays distinct segmental mobility[12,13,36−40] and mechanical properties.[41] The DIL segmental dynamics is found to be slower than that in the bulk, with a slowing down that is significantly enhanced when decreasing the polymer molecular weight (MW).[13,41] It has been suggested that long chains form a layer with frustrated chain packing leading to a lower density than the density of the bulk polymer matrix, whereas short chains can pack better at the interface. Additional indications for the reduction in mass density with increasing MW in the presence of the hard NP surfaces have been provided by pycnometry measurements.[13,41]

At the present stage, the characteristics of static interfacial layers of reduced density are thus mostly unknown. For instance, the thickness of the dynamic interfacial layer has been found to increase with decreasing temperature,[12] while the temperature dependence of its static counterpart remains unidentified. Elucidating these issues requires controlling the dispersion state of the NPs, in order to diminish the influence of the interparticle structure factor, and possibly eliminate it. Here we demonstrate that under ideal dispersion conditions a static interfacial layer can be evidenced by small-angle scattering and numerical modeling, and its evolution with annealing can be studied. In addition, we use SANS to characterize the conformation of polymer chains, and provide simultaneously an analysis of the stability of the preadsorbed layer during film formation and annealing. To achieve these goals, the particle dispersion of different nanocomposite formulations based on poly(vinyl acetate) (PVAc) and silica NPs is carefully investigated, comparing systems with polymer preadsorption to a reference system referred to as "bare" (i.e., NPs without any coating) throughout this article. The different formulations with bare and preadsorbed NPs are illustrated in Scheme 1.

Scheme 1. Influence of Chain Preadsorption (thin or thick polymer layer), Casting Speed (fast or slow), Chain Mass, and Annealing on Nanocomposite Structure

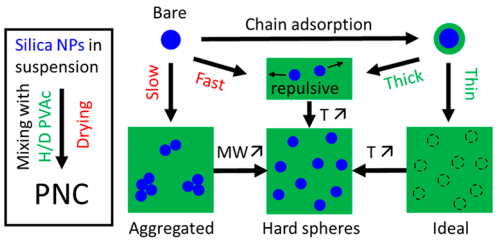

2. RESULTS AND DISCUSSION

2.1. Tuning PNC Filler Dispersion. In this study, we formulated an intermediate concentration of silica NPs, Φ_{NP} of ca. 9 vol %, to limit the influence of the structure factor caused by particle−particle correlations and have sufficient scattering signal. Several hydrogenated and deuterated PVAc polymers have been used in our study, with the samples named H*X* (hydrogenated) or D*X* (deuterated), with *X* indicating molecular weight in kg/mol (see Table 1). Sample identification is coded in the following way: the first part describes the nanoparticles either preadsorbed with the polymer or bare, while the second part presents the polymer matrix in which these NPs are dispersed. As an example, the H40(25%)@H10/D10 sample is nanoparticles preadsorbed with hydrogenated polymer MW ≈ 40 kg/mol at 25 wt % (measured by TGA) and dissolved in a polymer matrix that is a

DOI: 10.1021/acsami.9b04553
ACS Appl. Mater. Interfaces 2019, 11, 17863−17872

Table 1. Characteristics of the Protonated (H) and Deuterated (D) PVAc[a]

Name	MW(kg/mol)	PI	R_g (nm)
H10	10.6	1.2	2.7
D10	13.3	1.1	3.0
H20	19.6	1.3	3.7
H39	38.7	1.2	5.0
H40	41.0	2.4	5.2
H113	113.0	1.3	8.7
H240	242.7	2.7	10.8

[a]MW is the weight-average molecular weight and PDI the polydispersity. H39, H40, and H240 are commercial products from Polymer Source Inc., Alfa Aesar, and Scientific Polymer Product Inc., respectively.

blend of protonated and deuterated chains with MW ≈ 10 kg/mol under the zero average contrast condition (ZAC, matching the NPs with neutrons, see SI).[42,43] Bare H40/D10 means a sample with bare NPs dispersed in a fully deuterated polymer matrix with MW ≈ 10 kg/mol. Samples are summarized in Table 2 where the adsorbed TGA fractions have been converted in thickness estimates. Four SAXS intensity curves are shown in Figure 1: two for preadsorbed (H40) NPs in matrices with different deuteration schemes (D10 or H10/D10) but otherwise identical polymer, and two for the bare reference system with different drying speeds, fast or slow. The preadsorbed samples are always dried slowly. The natural contrast of X-rays provides silica scattering only and, due to the insensitivity of X-rays to deuteration, both preadsorbed systems display virtually identical structures. The scattered intensity of monodisperse and spherical silica beads in the polymer reads:

$$I(q) = \Phi_{NP}\Delta\rho^2 V_{NP} S(q) P(q) \quad (1)$$

where $\Delta\rho$ is the contrast between silica and the PVAc matrix, V_{NP} the NP volume, $S(q)$ the static structure factor, and $P(q)$ the particle form factor. $P(q)$ describes the scattering from isolated NPs with a Guinier plateau region at low q, which relates data to the particle R_g ($I(q) \propto \exp[-q^2R_g^2/3]$), and a Porod regime associated with scattering of the local interface and defined by a power law in the high-q range (q^{-4} for a smooth surface). $S(q)$ describes the correlations between NPs, and a low-q intensity increase (instead of the low-q plateau) usually indicates aggregation. The latter is accompanied by a depression of the intensity with respect to $P(q)$ at intermediate

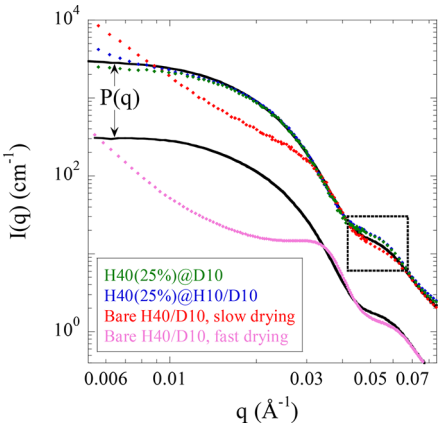

Figure 1. SAXS intensities of PNCs with preadsorbed layer (H40, 25%) normalized to NP form factor $P(q)$ in H10/D10 matrix and D10 matrix, respectively, compared to bare PNC-system (H40/D10) with slow and fast drying. The latter has been shifted for clarity (×0.1). $P(q)$ is measured in ethanol (0.7 vol %).

q, termed correlation hole. Note that adding polydispersity in size for the nanoparticles requires one to weight properly each partial correlation by the proper mass and the use of a simple product in eq 1 is no more valid,[27,35] but in the case of the absence of structure the scattered intensity is reduced to an average over the polydisperse form factor scattering, as done here.

The scattered intensities for the preadsorbed samples in Figure 1 show a close agreement with $P(q)$ measured independently in diluted solution (black solid line). Such a result suggests that these particles are ideally well-dispersed, and interactions between particles have been screened. This must be due to the presence of the preadsorbed layer, which sterically stabilizes the particles in solution and melt during film formation, and effectively screens hard sphere interactions leading to $S(q) \approx 1$. At intermediate to high q, however, the scattering differs from the form factor, around the form factor oscillation (see dashed box). One may note that both at higher and lower q, the agreement with $P(q)$ becomes again remarkable, indicating that the observed deviation cannot be an artifact caused by imperfect background subtractions. This modified form factor oscillation can be linked to the presence of an interfacial layer of polymer density different from the bulk, and a detailed description will be given below.

If one does not preadsorb the H40 chains, but incorporates them into the PNC matrix which becomes a mixture of H40/

Table 2. Samples Characteristics[a]

Code	D-PVAc in matrix (wt %)	Φ_{NP} (vol %)	Adsorbed chains	Amount of adsorbed chains (wt %)	Dry thickness (nm)
H15(53%)@D10	100	5.4	H15	53	4.0
H40(25%)@D10	100	8.7	H40	25	1.2
H40(25%)@H10/D10	39	9.5	H40	25	1.2
H40(25%)@D10	100	8.7	H40	25	1.2
H40(13%)@D10	100	8.3	H40	13	0.5
Bare H20/D10	39	8.3			
Bare H39/D10	39	9.1			
Bare H40/D10	39	8.7			
Bare H113/D10	39	8.3			
Bare H240/D10	39	5.6			

[a]The adsorbed chain fraction is given with respect to the mass of surface-modified NPs. The dry thickness is calculated using the bulk density for PVAc (1.25 g/cm^3).

DOI: 10.1021/acsami.9b04553
ACS Appl. Mater. Interfaces 2019, 11, 17863−17872

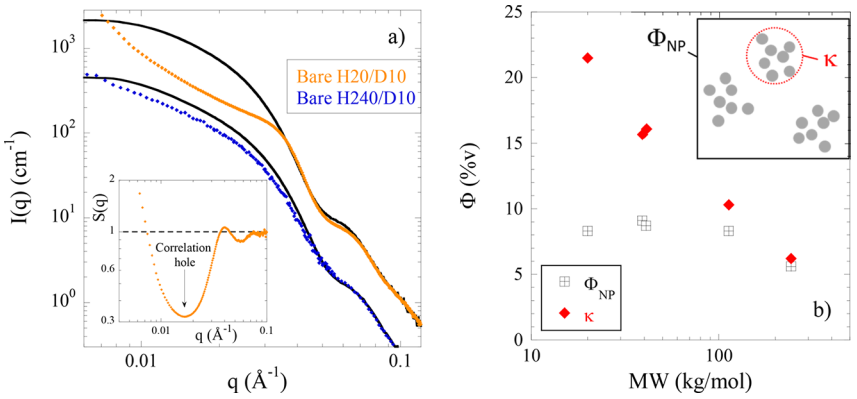

Figure 2. (a) SAXS intensities of bare PNC systems H20/D10 and H240/D10 compared to their respective form factor. The comparison for H240/D10 has been shifted for clarity (×0.2). (Inset) Apparent structure factor for bare H20/D10. (b) Silica volume fraction Φ_{NP} and compacity κ versus MW of the protonated chains in bare PNCs.

D10 chains with 39 vol % of 10 kg/mol chains, a sample of the bare system is formed. The higher intensity curve in Figure 1 corresponds to this sample dried slowly, as the two samples with preadsorbed chains. However, the SAXS curves differ strongly: the presence of a correlation hole around 0.02 Å^{-1} is caused by a repulsive structure factor indicating high local NP concentrations or aggregation. Moreover, in the q-range indicated by the dashed box, the intensity now passes below the form factor.

On the contrary, the lower intensity curve corresponds to a bare system which has undergone fast drying. Then, the long-range repulsive interactions of electrostatic origin in suspension are frozen in, and the system presents a repulsive peak at $q = \pi/R \approx 0.03$ Å^{-1}, corresponding to interparticle contact and thus aggregation. We will see below that such a strong repulsion can also be induced by very thick adsorbed steric layers, which induce ordering during drying due to high space-filling. Remarkably, a low-q upturn is also measured. Such a feature (also visible for the bare sample) is usually interpreted as large-scale heterogeneity in particle density, which may be due to aggregation, but can also be caused by large-scale modulations around the average local density. As with the aggregated bare PNC, the oscillation in the q-range of the dashed box for fast drying is again below the form factor. In this case, it is impossible to match the intensities simultaneously below and above this oscillation. The presence of a structure factor, either repulsive or aggregated, with possible higher order oscillations thus dominates the scattering signature in this region. This makes the analysis of the form factor oscillation difficult if not impossible. In any case, the SAXS data in Figure 1 clearly demonstrate ideal dispersion for PNCs with preadsorbed chains, while they reveal significant aggregation in PNCs with bare NPs, regardless of fast or slow drying. The same results for samples of different chain mass are presented in the SI.

Once these PNCs are formed, one may question their thermal stability. The evolution of the aggregated bare PNC (Figure 1) with temperature and annealing time (successively 96 °C, 145 °C, 9 days each and finally 180 °C for 9 h) has been studied by SAXS and the data are reported in the SI. The corresponding intensity curves are shown to be superimposed, indicating that once aggregated, the system does not evolve any further at the selected temperatures. PNCs with preadsorption are discussed below.

The annealing study of the bare PNCs suggests that the samples reached a steady state of aggregation during film formation. The dispersion in suspension was nonaggregated, as probed by freezing this state using the fast drying procedure, cf. Figure 1. There is thus an evolution toward aggregation, a kinetic process which should be influenced by the viscosity of the system. We have therefore varied systematically the mass of the protonated matrix polymer of the bare system, up to 240 kg/mol, while keeping constant the fraction and mass of the minority deuterated chains (10 kg/mol). The resulting state of dispersion of the aggregated bare PNCs is found to depend on the polymer molecular weight: two examples are shown in Figure 2a (see the SI for the others). The state of aggregation has been analyzed quantitatively using the apparent structure factor obtained by dividing the intensity by the average form factor as shown for the H20/D10-sample in the inset of Figure 2a. As mentioned above, this structure factor possesses a characteristic scattering signature, the correlation hole, and we have applied a recently proposed model[44] based on the depth of the correlation hole observed around 0.02 Å^{-1}. The latter is defined by the low-q limit of $S(q)$, which tends toward the (relative) isothermal compressibility and reflects, therefore, a concentration effect on local scale. Our analysis reveals aggregation of the NPs in the PNC corresponding to aggregates of internal density approximately $\kappa = 21.5\%$. For comparison, κ equals 6.2% for the H240/D10 PNC. Given that the silica volume fractions of these two samples determined by TGA are 8.3 and 5.6 vol %, respectively, the large κ value obtained for the former indicates a nonhomogeneous dispersion, i.e., the formation of zones denser than the average nanocomposite, which we identify with aggregates, as shown in the inset of Figure 2b. On the other hand, κ approaching the total silica volume fraction for the second sample ($\kappa \approx \Phi_{NP}$) indicates a homogeneous, nonaggregated hard-sphere dispersion.

The complete series of intensity curves of bare samples as shown in the SI indicates that the quality of dispersion increases in a systematic manner with the matrix chain mass. As shown in Figure 2a, the intensity around 0.02 Å^{-1} approaches the form factor, i.e., the correlation hole is closed indicating almost individual dispersion, and the resulting κ decreases down to Φ_{NP}. This evolution is presented in Figure 2b. It is in line with a previous study of the quality of dispersion as a function of molecular weight in a silica−latex system:[28] the polymer with the highest MW increases

DOI: 10.1021/acsami.9b04553
ACS Appl. Mater. Interfaces 2019, 11, 17863−17872

considerably the viscosity, thus keeping the system from approaching an aggregated state of lower free energy. Note that the lowest MW sample, 10 kg/mol, presents signs of phase separation and could not be measured reliably. Also, two similar samples have been measured (H39/D10 and H40/D10), showing robustness of the analysis of Figure 2b.

Summarizing the different interactions between NPs during film formation and in PNCs, it is noted that NPs are originally stabilized by long-range electrostatic repulsion in solution, a state which can be quenched by fast drying avoiding aggregation that would result from the formation of strong hydrogen bonds between the surface silanol groups of silica NPs. During slow film formation, particles may be stabilized by a steric preadsorbed layer of the same chemical nature as the matrix and favored by hydrogen bonding between the silanols and the carbonyl groups of PVAc.[22] This leads to a screening effect where the repulsive hard sphere interactions are compensated by attraction, and the resulting dispersion is ideal form factor scattering, in analogy with ideal polymer statistics in Θ-solvent. For nanoparticles, reaching this ideal case is the primary goal of this article: slight variations of the form factor, e.g., by surrounding matrix polymer density modifications evidenced below, can be then measured. Without preadsorption, NPs aggregate, which can be prevented by increasing the matrix viscosity with long chains, leading to a hard sphere dispersion without aggregation. In return, decreasing the matrix chain MW leads to aggregation, i.e., the formation of zones denser than the particle volume fraction ($\kappa > \Phi_{NP}$).

2.2. Evolution of Preadsorbed PNCs with Annealing. The structure of the PNCs made of NPs with polymer preadsorption was found to be ideally well-dispersed at room temperature (RT) after film formation as shown in Figure 1, with screened hard sphere interactions, i.e., a structure factor approaching one. In Figure 3a, the SAXS intensities after

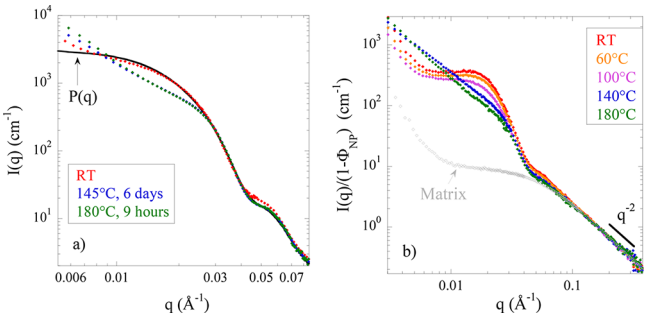

Figure 3. Annealing of systems with preadsorbed NPs. (a) SAXS intensities of H40(25%)@H10/D10. (b) SANS intensities of H15(53%)@D10, annealing time 1.5 h at each temperature. RT corresponds to samples without annealing measured at room temperature.

annealing under vacuum such a sample (H40(25%)@H10/D10) during 6 days at 145 °C, and an additional 9 h at 180 °C are presented. They clearly show the formation of a correlation hole around 0.02 Å^{-1}, accompanied by a low-q increase, both indicating the onset of interparticle interactions. Judging from the superposition of the intensity in the correlation hole, most of the process seems to have taken place already at the lower temperature. The resulting local particle density in these aggregates deduced from the depth of the correlation hole is κ = 9.5%, i.e., exactly the silica volume fraction given by TGA (Φ_{NP} = 9.5%): particles explore space due to the higher mobility during annealing, and adopt a well-dispersed particle configuration governed by hard sphere interactions. The system thus loses the screening of the interactions. As we suspect the steric stabilization layer to be responsible of the initial screening, the loss of screening with annealing suggests that the steric stabilization layer has disappeared during annealing, or during the last stages of film formation, when the NP configuration is already set. This is to be expected for mobile chains, as mixing with the matrix chains is entropically favorable. On the other hand, further aggregation is not promoted by annealing, presumably because the interactions of the polymer with the Si−OH groups of the particles are attractive enough to form a bound layer and to impede direct silica−silica contact.

In Figure 3b, the evolution of dispersion of a PNC with a thicker preadsorbed layer (H15(53%)@D10, 53% corresponding to 4 nm) is shown. In this system with a deuterated polymer matrix, the measurements could be made by SANS due to the strong contrast of the silica in the matrix. The dispersion of the silica in the PNCs observed in Figure 3b resembles the one obtained by fast drying in the absence of preadsorption, see Figure 1. This shows that fast drying is one possibility to freeze a structure, i.e., strong repulsion in suspension, but that thick enough preadsorbed polymer layers may induce sufficient steric repulsion, too. Indeed, in solution the dry thickness of 4 nm may swell considerably, as discussed by Jouault et al.[34] A swelling by a factor of 2 corresponding to a 50% solvent (during film formation) or matrix polymer (in the PNC) concentration in the layer would increase the nominal silica radius by almost a factor of 2, thus increasing the effective particle volume fraction by a factor of 8. Already in early stages of drying a strong steric ordering is thus to be expected, resulting in a dominant structure factor peak in PNCs as observed in Figure 3b around q = 0.02 Å^{-1}. More quantitatively, the position of this peak corresponds to a typical center-to-center interparticle distance of ca. 31 nm, indicating that NPs interact repulsively over surface-to-surface distances of about 10 nm, which is compatible with interacting swollen polymer layers in solution before film formation. In the PNC, the R_g for the 15 kg/mol chains is 3.2 nm, indicating that the polymer interphase is not confined, and no interactions are expected to be present maintaining the initial ordering in suspension. Therefore, upon annealing, the repulsive peak disappears and is replaced by a low-q upturn with correlation hole in the region of the peak. The depth of the correlation hole corresponds to a local particle volume fraction of κ = 10.8%, compatible with the nominal silica concentration and thus indicates that the dispersion of this sample remains good or at most weakly aggregated.

An additional advantage of the H/D-contrast is that the preadsorbed hydrogenated polymer should also be visible in the same intensity curves. If the preadsorbed layer remained dense, with a sharp interface to the matrix, then its scattering in the high-q range would be Porod-like, proportional to q^{-4}. This does not correspond to the observation in Figure 3b, providing experimental evidence for the aforementioned supposition of chain desorption in the final PNC: instead of the expected Porod-like behavior, Debye-like chain scattering proportional to q^{-2} is found, similar to a pure matrix containing both H and D polymers. For comparison, the scattering of a compositionally close H10/D10 matrix is superimposed in Figure 3b. This shows that individual preadsorbed H15-chains have gained

DOI: 10.1021/acsami.9b04553
ACS Appl. Mater. Interfaces 2019, 11, 17863−17872

visibility by mixing with the D10-matrix chains, either by interpenetration or by completely desorbing into the matrix.

For both cases discussed in Figure 3, either with a thin or thick preadsorbed layer, and different contrast conditions for SAXS and SANS, the evolution of the curves provides indications for desorption of a preadsorbed layer under thermal annealing. The particle interactions change, with a saturation setting in above 140 °C. For both types of samples, however, it is unclear if the layer has already disappeared in the late stages of film formation, and aggregation or loss of screening are triggered by thermal energy during annealing, or if the annealing stage is responsible for removing the preadsorbed layer. There is an indication in favor of the first option in Figure 3b: the chain scattering at high-q does not seem to evolve with annealing, suggesting that a static state of chain distribution in the matrix has been reached already before annealing, i.e., during film formation. A combined SAXS and SANS experiment with modeling of the polymer density in the region of the preadsorbed layers will answer this question in the next section.

2.3. Determination of Polymer Density Gradient at the NP Surface. Up to here, states of ideal NP dispersion have been prepared and identified by scattering, providing now unique access to the structure of the interfacial layer. In the high-q range in Figure 1 illustrated by the dashed box around 0.05 Å^{-1}, a small but measurable additional SAXS intensity is observed in the oscillation of samples with preadsorption with respect to the form factor. The latter has been measured in solvent and without polymer, i.e., it corresponds to a molecularly smooth contrast situation. As the silica is the same in all cases, as well as the bulk polymer, this suggests the presence of a structurally different interfacial layer which is particularly visible in systems with preadsorption, due to the good dispersion which minimizes the influence of the structure factor. Such a layer located just outside the particle naturally affects the form factor oscillation in this q-range. Moreover, the increase in intensity corresponds to an increase in contrast between silica and the surrounding layer, i.e., a decrease in the density of the polymer layer, as there is only one contrasted polymer species with respect to the (unchanged) silica in SAXS.

To investigate this point further, we have performed numerical simulations of form factors of the same silica NPs surrounded by a spherically symmetric layer of modified density of arbitrary profile, adapting a model recently developed for microgel particles in aqueous suspension.[45] Form-free multishell Monte Carlo simulations (reverse Monte Carlo, RMC, as described in the SI) allow reproducing perfectly the experimental intensity curves as shown in Figure 4, and the resulting density profile is shown in the inset. It presents a depleted layer of reduced density by ca. 10%, with a maximum extension of 2 nm, and a progressive transition to the bulk density, i.e., a density gradient. This thickness is larger than the one of the dry layer of 1.2 nm, and smaller than the chain radius of gyration of 5 nm. The chain packing is thus perturbed only in the close vicinity of the interface, and the parts extending into the matrix adopt the density and conformations of neat polymer. Moreover, the same result of 2 nm is found for four samples of the preadsorbed systems with dry layer thicknesses measured by TGA of 0.5 and 1.2 nm, indicating that the range of the gradient is found to be independent of the initial thickness of the adsorbed layer (see the SI). The gradient is also robust with respect to the type of

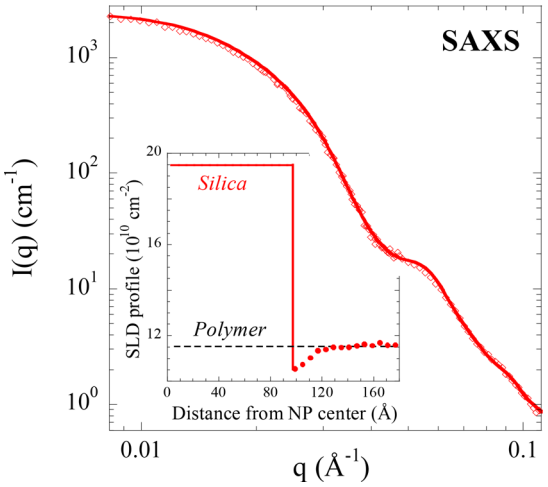

Figure 4. Comparison of SAXS intensity of PNC H40(25%)@D10 with preadsorbed layer intensity to numerical modeling. (Inset) Resulting multishell form-free profile determined by RMC.

matrix chains (see the SI). The interfacial layers are thus generated by short-range interactions with the interface. These layers can therefore not be identified with the preadsorbed ones, but they can be observed best in the ideal dispersion triggered by preadsorbed layers. They are probably caused by reduced packing of adsorbed chains close to the NP surface. Interestingly, the gradient is not observed for preadsorbed chains of low mass (10 kg/mol, data shown in the SI). As discussed by Cheng et al.,[13] the short chains close to the NP surface are expected to adjust their conformation more easily than long ones, leading to a homogeneous density throughout the PNC. Moreover, no evidence for a static interfacial layer is found with hard sphere dispersions of bare NPs as shown in Figure 2a. This suggests that only the packing and folding properties of adsorbed chains in suspension induce layers of reduced density. To the best of our knowledge, this is the first observation of a static polymer density gradient on the filler surface, evidenced by a combination of SAXS and numerical simulations, under conditions of ideal dispersion allowing a full treatment of particle polydispersity, without uncontrolled approximations introduced by the structure factor.

The interfacial density gradient which is linked to the shape of the form factor oscillation seems to evolve with annealing in Figure 3a: the difference with respect to the pure particle form factor is found to disappear, while the superposition of the intensity at higher and lower q values remains remarkable, due to the absence of aggregation. This demonstrates a reorganization of the local polymer structure close to the interface, tending toward a homogeneous polymer density. The latter must be linked to chain folding, which can be different directly after film formation, presumably because the interface is still solvated in the late stages of drying and allows for chain rearrangements. As a result, the static properties of the polymer layer before annealing in the PNCs show the presence of a weak density gradient as measured and modeled in Figure 4. The weakness of this gradient contrasts with the well-established dynamical properties of the polymer layer surrounding NPs as discussed in the introduction.[12] One of the main conclusions of this work is thus the characterization of the polymer density gradient at room temperature, and its thermal evolution: the static interfacial layer disappears with annealing. We have additional SANS measurements (see the

DOI: 10.1021/acsami.9b04553
ACS Appl. Mater. Interfaces 2019, 11, 17863−17872

SI) which show that the H/D blend of the sample of Figure 3a tends to demix at high temperature, following spinodal decomposition due to a non-zero Flory interaction parameter (χN). This proves that the polymer matrix undergoes rearrangements, allowing simultaneously the interfacial layer to reach the same density as the bulk.

In the first section of this article, we have shown the dominant influence of preadsorbed chains on the dispersion of NPs in PNCs, and provided evidence for layer desorption, presumably in the late stages of film formation, followed by changes in particle interactions upon annealing. Only in the presence of ideally well-dispersed filler NPs stabilized during film formation by preadsorbed chains, a static interfacial layer of reduced polymer density is visible in the scattering, and its characterization presents the key result of this article. In this final part, we now use SANS with deuteration to verify the presence or absence of the preadsorbed layer directly after film formation. In Figure 5, the neutron scattering of the

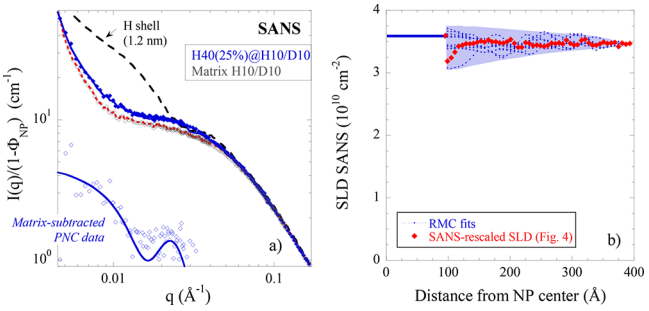

Figure 5. (a) SANS intensities of PNC H40(25%)@H10/D10 (Φ_{NP} = 9.5 vol %, blue plain symbols) and the pure matrix H10/D10 (gray empty symbols). Data are compared to the pure matrix contribution added to calculated scattered intensities of either a homogeneously protonated preadsorbed shell (thickness = 1.2 nm, dashed line), of a shell of reduced density but no isotopic contrast as obtained from SAXS and shown in the inset of Figure 4 (red dotted line), and of an isotopic profile determined by RMC (blue solid line). The lower intensity (blue empty symbols) corresponds to the PNC data after subtraction of the matrix contribution. (b) Envelope of family of SANS SLD profiles (blue) determined by RMC compared to rescaled SAXS reduced-density profile (red).

H40(25%)@H10/D10 sample at room temperature, after film formation (no annealing), is presented. Note that the SAXS intensity of the same sample is shown in Figure 1.

In the SANS case, due to the mixture of H and D chains (61%H/39%D), the silica is contrast-matched, and only the contribution of the polymer chains is visible. At high q, the chain form factor is thus retrieved, and it can indeed be superimposed as shown in the pure matrix scattering rescaled according to composition. The good high-q superposition also indicates that the chain conformations are not modified within the PNC, and so are their radii of gyration, which remain much bigger than the thickness of the dry adsorbed layer. Moreover, if the hydrogenated preadsorbed chains formed a dense layer of the same dry thickness as the one found by TGA, then the calculated dashed black curve would be measured. Clearly this is not the case, proving that the preadsorbed layer has disappeared in the late stages of film formation, whereas it must have been present in the early stages to ensure colloidal stability and screening of interactions. One might wonder if the layer may still partially persist, but the big difference between the H-shell prediction and the measured intensity on the logarithmic scale suggests at most a very small residue. On the opposite side, using the density profile obtained by SAXS (Figure 4 and red curve in Figure 5b) yields a too low intensity, and does not allow reproducing the experimental SANS intensity (see red dotted line in Figure 5a).

In the PNC measurement in Figure 5a, there is a small but clearly identified additional contribution observable in the intermediate-q range, between 0.01 and 0.03 Å^{-1}. This contribution could be modeled using the same numerical approach as above, the free-form RMC, and the resulting average intensity over many Monte Carlo runs is plotted in Figure 5a (solid line). By construction, it is found to fit the experimentally observed intensity. As the experiment is a SANS measurement, the resulting density profile corresponds to an H/D-contrast. The additional signal (on top of matrix scattering) in Figure 5a, however, is so small that this profile could not be determined unambiguously: there is no clear H- or D-enrichment close to the interface. A variety of profiles can be generated, all in an error-bar around a scattering length density (SLD) of the silica and the contrast matching polymer. Several of these profiles have been superimposed in Figure 5b, illustrating that H/D-modulations are present but very small. To illustrate the outcome of the simulations, we have therefore drawn their envelope. Each curve taken individually shows some small fluctuations within this envelope, but their exact position appears to be random. A possible interpretation is that indeed minor H- and D-fluctuations persist, but that they are different around each NP. As a final result, virtually all of the preadsorbed H-polymer has been mixed with the matrix polymer, and this result does not depend on the masses of preadsorbed chains (10 or 40 kg/mol, see the SI).

3. CONCLUSIONS

The filler dispersion and the structure of the polymer matrix of polymer nanocomposites have been studied using SAXS and SANS, with a particular focus on the characterization of a static interfacial polymer layer of lower density which is possible to be observed only in ideal dispersions. A form-free model has been applied to the SAXS data of ideally dispersed NPs, showing that the reduced polymer density, by ca. 10%, extends over approximately 2 nm from the particle surface, reaching smoothly the bulk density. This is less than the polymer radius of gyration, indicating that only parts of the molecules very close to the surface cannot pack ideally. Moreover, the resulting density gradient has been shown to be compatible with the SANS data analysis, where only a very weak signal is measured. The SANS data are compatible with a combination of a mass density gradient and some very weak isotopic fluctuations. The thermal properties of this interfacial layer have been investigated by annealing, and the layer signature in the intermediate to high-q domain of the scattered intensity is shown to disappear. This suggests that local rearrangements of the chains allow relaxation of thermodynamically frozen and unfavorable states of chain packing and folding, filling the interfacial layer up to the matrix density. Note that the required chain mobility at high temperature is demonstrated independently by SANS through the signature of the onset of a H/D-phase separation. In parallel, the filler structure evolves toward a hard sphere dispersion during annealing, i.e., the screening effect of the preadsorbed layer disappears. We have then shown by SANS compared to a model calculation that this is accompanied by the quasi-total desorption of the

DOI: 10.1021/acsami.9b04553
ACS Appl. Mater. Interfaces 2019, 11, 17863−17872

preadsorbed layer already in samples dried at room temperature.

Controlling the dispersion state of the PNCs has been demonstrated to be crucial for the observation of the static interfacial layer. Indeed, the additional intensity caused by the interfacial layer can only be attributed unambiguously to the layer if the structure factor is weak in the same q range. Our approach is to require good agreement between the particle form factor and the PNC intensity both above and below the form factor oscillation. This is the case for ideally dispersed NPs obtained with polymer preadsorption, which tends to screen the repulsive hard sphere interactions. It is important to realize that the same interfacial layer is found for preadsorbed layers of different dry thickness, and in different matrices, by SAXS or SANS: thus the preadsorbed and the interfacial layers are of different nature. The static interfacial layer is characterized by a density gradient which is caused by imperfect chain packing and folding close to the NP interface of the preadsorbed polymer in suspension, but does not encompass the entire adsorbed layer. It is not observed for short preadsorbed chains, which reveals a dependence of the interfacial layer density on the molecular weight, in agreement with previous studies.[13]

Our findings thus contribute to the understanding of polymer-mediated structure formation in PNCs, and in particular characterize for the first time static interfacial effects affecting the density and thus dynamical and mechanical properties of such materials, as a function of dispersion, using a combination of X-ray scattering and simulations. Our article specifies the exact conditions of observation and existence of a gradient in the static layer of reduced density. In parallel, small-angle neutron scattering of the same samples has been shown to provide insight into chain conformations and thermal stability of preadsorbed layers. Detailed studies of layer and polymer conformations are currently being performed, and they shall deepen our knowledge of how chains arrange around NPs and how they mediate particle interactions and thus macroscopic properties like mechanical reinforcement in polymer nanocomposites.

4. EXPERIMENTAL SECTION

4.1. Synthesis of Silica Nanoparticles. Different batches of spherical silica NPs were synthesized by a modified Stöber method[46] in ethanol where they are electrostatically stabilized, with a final NP concentration of 16 mg/mL. They have been characterized by SAXS in ethanol at 0.7 vol % dilution. For each batch, the scattered intensity revealed a log-normal size distribution with polydispersity about 18% and an average NP radius of ca. 10 nm (see the SI for details).

4.2. Synthesis of PVAc. Full details on synthesis procedure are given in the SI. In short, poly(vinyl acetate) was synthesized via reversible addition−fragmentation chain transfer (RAFT) polymerization. Vinyl acetate monomer, cyanomethyl methyl(4-pyridyl)-carbamodithioate (CTA, Sigma), and azobis(isobutyronitrile) (AIBN, Sigma) were dissolved in ethyl acetate (1:2 mass ratio, vinyl acetate:ethyl acetate). The monomer solution was heated to 76 °C and stirred for 48 h for the protonated monomer and 72 h for the deuterated monomer, followed by purification by precipitation cycles from tetrahydrofuran (THF) into hexane. Sample purity was confirmed by ^{1}H nuclear magnetic resonance (NMR) spectra by a Bruker 400 MHz NMR spectrometer using $CDCl_3$. Molecular weights were obtained by size exclusion chromatography at 25 °C in THF (Agilent 1310B 1260 Infinity Isocratic HPLC). (Certain commercial equipment, instruments, or materials are identified in this paper to foster understanding. Such identification does not imply recommendation or endorsement by the National Institute of Standards and Technology, nor does it imply that the materials or equipment identified are necessarily the best available for the purpose.) The radii of gyration of the different polymer chains in the bulk polymer have been determined by SANS in pure H/D matrices. Results are summarized in Table 1.

4.3. Preparation of Preadsorbed NPs. PVAc layers have been preadsorbed by mixing and stirring appropriate amounts of polymer in methyl ether ketone (MEK, ACS-grade, BDH VWR) with silica nanoparticles suspended in ethanol (Sigma-Aldrich, ≥99.5%) during 12 h. The silica concentration was kept constant with 3.2 mg/mL, whereas the polymer concentration was varied from 5 to 27 mg/mL. Samples were then centrifuged (total volume 20 mL, 12 000 rotations per minute, 30 min, repeated 3 times), followed each time by redispersion in MEK. In the case of the highest adsorption, dialysis versus MEK (cutoff 50 kDa, 3 days) was used instead of centrifugation to remove the free polymer.

The system formulation parameters are given by the mass of the preadsorbed chains and the matrix chains. The amount of adsorbed polymer was determined by thermogravimetric analysis and is reported together with the formulation parameters in Table 2. The corresponding dry nanometric thickness of the layer was estimated using the bulk density of the neat polymer, and the result is also reported in the table. The reference system without a preadsorbed layer is called "bare" throughout this article, and both systems are illustrated in Scheme 1.

4.4. Formulation of Polymer Nanocomposites. The polymers dissolved in MEK and either bare or preadsorbed NPs in ethanol were mixed with the proportions calculated to obtain a nominal silica content of 9 vol % in the final PNCs. After 12 h of mixing, the solvent was evaporated, thus forming nanocomposites. Depending on the drying procedure, with or without vacuum for evaporation of virtually all solvent, the drying process was fast or slow. Slow drying was obtained by progressive casting over 1 day, whereas fast drying was almost instantaneous and corresponded to rapid solvent evaporation under vacuum. Both procedures were completed by 3 days under vacuum. The different formulation routes are illustrated in Scheme 1.

4.5. Thermogravimetric Analysis. Exact loadings of our PNCs were determined by TGA (TA Discovery, 20 °C/min, under air) from the weight loss between 200 and 900 °C. The silica volume fraction, Φ_{NP}, was determined by mass conservation using the densities of neat PVAc and silica obtained by SANS. For preadsorbed NPs, the adsorbed amount of PVAc on silica was obtained using a 5 °C/min heating rate after a 20 min isotherm at 100 °C.

4.6. Structural Analysis. Part of the SAXS experiments were performed with an in-house setup of the Laboratoire Charles Coulomb, "Réseau X et gamma", University of Montpellier, France. A high-brightness low-power X-ray tube, coupled with aspheric multilayer optics (GeniX3D from Xenocs), was employed. It delivers an ultralow divergent beam (0.5 mrad). We worked in a transmission configuration, and scattered intensities were measured by a two-dimensional "Pilatus" pixel detector at a single sample-to-detector distance D = 1900 mm, leading to a q range from 5.5×10^{-3} to 0.2 Å^{-1}. Other SAXS experiments were conducted using a SAXSLab Ganesha at the Shared Materials Instrumentation Facility (SMIF), Duke University, North Carolina. A Xenocs GeniX3D microfocus source was employed with a copper target leading to a monochromatic beam with wavelength λ = 1.54 Å. We worked in transmission geometry with two distances D = 1491 and 441 mm giving a total q range from 3.5×10^{-3} to 0.6 Å^{-1}. The scattering cross section per unit sample volume $d\Sigma/d\Omega$ (in cm^{-1}), which we term scattered intensity $I(q)$, was obtained by using standard procedures including background subtraction and calibration.[35]

4.7. SANS and Deuteration Schemes. SANS experiments were carried out on the NGB 30 m beamline[47] at the National Institute of Standards and Technology Center for Neutron Research (NCNR) in Gaithersburg (MD, USA). Some measurements were also carried out on GP-SANS at the High Flux Isotope Reactor (HFIR) at Oak Ridge National Laboratory (ORNL, USA). We used different configurations covering a q range from ca. 3×10^{-3} to 0.45 Å^{-1}. NGB: D = 13.17 m, 4 and 1.33 m, all λ = 6 Å, and GP-SANS: D = 19.2 m, 6.8 and 1.8 m,

DOI: 10.1021/acsami.9b04553
ACS Appl. Mater. Interfaces 2019, 11, 17863−17872

all λ = 4.75 Å. PNC samples with a thickness of ca. 0.25 mm were mounted between two quartz windows. Empty cell subtraction, calibration by 1 mm light water in Hellma cuvette, and absolute determination of scattering cross sections were performed using standard procedures.[48] For in situ temperature measurements on NGB, we used a 7 position heating block (7HB, ±1 °C of precision) with a continuous nitrogen flow. Contrast variation in solvents was used to determine the neutron scattering length densities and thus also the densities in solution in g/cm^3 used for the calculation of the volume fractions, Φ_{NP}. These measurements were performed at HFIR. For the silica in mixtures of H- and D6-ethanol after dialysis against ethanol, the SLD was found to be $\rho_{SiO2} = 3.59 \times 10^{10}$ cm^{-2} (2.27 g/cm^3); for the H-PVAc (10 kg/mol) in H- and D6-acetone, $\rho_H = 1.38 \times 10^{10}$ cm^{-2} (1.25 g/cm^3); and finally for D-PVAc (10 kg/mol), $\rho_D = 7.02 \times 10^{10}$ cm^{-2} (1.37 g/cm^3). Contrast variation experiments are reported in the SI.

By formulating nanocomposites with fully deuterated matrix chains (nominal MW = 10 kg/mol termed D10), the contribution of the hydrogenated preadsorbed chains may be measured by SANS. Finally, by substituting only a fraction (61%H following the above contrast variations) of the matrix chains with protonated chains, the silica NPs can be contrast matched (zero average contrast,[42,43] see the SI), and both the preadsorbed chains and the matrix chains can be observed by SANS.

■ ASSOCIATED CONTENT

Supporting Information

The Supporting Information is available free of charge on the ACS Publications website at DOI: 10.1021/acsami.9b04553.

Characterization of silica nanoparticles, synthesis of PVAc, contrast variation experiments, impact of MW and annealing on the filler dispersion of bare NPs in PNC, RMC algorithm for the determination of the polymer density profile at the NP interface, impact of the preadsorbed layer and matrix, and impact of annealing on H/D blends (PDF)

■ AUTHOR INFORMATION

Corresponding Authors

*E-mail: anne-caroline.genix@umontpellier.fr (A.-C.G.).
*E-mail: bocharovav@ornl.gov (V.B.).

ORCID

Anne-Caroline Genix: 0000-0003-0529-7205
Vera Bocharova: 0000-0003-4270-3866
Bobby Carroll: 0000-0002-0536-9734
Tomonori Saito: 0000-0002-4536-7530
Lilin He: 0000-0002-9560-8101
Alexei P. Sokolov: 0000-0002-8187-9445
Julian Oberdisse: 0000-0002-9510-1722

Notes

The authors declare no competing financial interest.

■ ACKNOWLEDGMENTS

This work was supported by the U.S. Department of Energy, Office of Science, Basic Energy Sciences, Materials Sciences and Engineering Division. A portion of this research used resources at the High Flux Isotope Reactor, a DOE Office of Science User Facility operated by the Oak Ridge National Laboratory. Access to the NBG 30 m SANS instrument was provided by the Center for High Resolution Neutron Scattering, a partnership between the National Institute of Standards and Technology and the National Science Foundation under Agreement No. DMR-1508249. A.-C.G. and J.O. are thankful for support by the ANR NANODYN project, Grant ANR-14-CE22-0001-01 of the French Agence Nationale de la Recherche. The authors are thankful to Dr. Konstantinos Misichronis for his help on polymer synthesis.

■ REFERENCES

(1) Yu, A.; Ramesh, P.; Itkis, M. E.; Bekyarova, E.; Haddon, R. C. Graphite Nanoplatelet−Epoxy Composite Thermal Interface Materials. *J. Phys. Chem. C* **2007**, *111* (21), 7565−7569.

(2) Jancar, J.; Douglas, J. F.; Starr, F. W.; Kumar, S. K.; Cassagnau, P.; Lesser, A. J.; Sternstein, S. S.; Buehler, M. J. Current Issues in Research on Structure-Property Relationships in Polymer Nanocomposites. *Polymer* **2010**, *51* (15), 3321−3343.

(3) Mittal, V.; Kim, J. K.; Pal, K. *Recent Adances in Elastomeric Nanocomposites*; Springer-Verlag: Berlin Heidelberg, 2011.

(4) Heinrich, G.; Kluppel, M.; Vilgis, T. A. Reinforcement of Elastomers. *Curr. Opin. Solid State Mater. Sci.* **2002**, *6* (3), 195−203.

(5) Zhao, D.; Ge, S.; Senses, E.; Akcora, P.; Jestin, J.; Kumar, S. K. Role of Filler Shape and Connectivity on the Viscoelastic Behavior in Polymer Nanocomposites. *Macromolecules* **2015**, *48* (15), 5433−5438.

(6) Baeza, G. P.; Oberdisse, J.; Alegria, A.; Couty, M.; Genix, A. C. A High-Temperature Dielectric Process as a Probe of Large-Scale Silica Filler Structure in Simplified Industrial Nanocomposites. *Phys. Chem. Chem. Phys.* **2015**, *17*, 1660−1666.

(7) Akcora, P.; Kumar, S. K.; Moll, J.; Lewis, S.; Schadler, L. S.; Li, Y.; Benicewicz, B. C.; Sandy, A.; Narayanan, S.; Ilavsky, J.; Thiyagarajan, P.; Colby, R. H.; Douglas, J. F. "Gel-Like" Mechanical Reinforcement in Polymer Nanocomposite Melts. *Macromolecules* **2010**, *43* (2), 1003−1010.

(8) Maillard, D.; Kumar, S. K.; Fragneaud, B.; Kysar, J. W.; Rungta, A.; Benicewicz, B. C.; Deng, H.; Brinson, L. C.; Douglas, J. F. Mechanical Properties of Thin Glassy Polymer Films Filled with Spherical Polymer-Grafted Nanoparticles. *Nano Lett.* **2012**, *12* (8), 3909−3914.

(9) Suematsu, K.; Arimura, M.; Uchiyama, N.; Saita, S. Transparent BaTiO3/PMMA Nanocomposite Films for Display Technologies: Facile Surface Modification Approach for BaTiO3 Nanoparticles. *ACS Applied Nano Materials* **2018**, *1* (5), 2430−2437.

(10) Voylov, D. N.; Holt, A. P.; Doughty, B.; Bocharova, V.; Meyer, H. M.; Cheng, S.; Martin, H.; Dadmun, M.; Kisliuk, A.; Sokolov, A. P. Unraveling the Molecular Weight Dependence of Interfacial Interactions in Poly(2-Vinylpyridine)/Silica Nanocomposites. *ACS Macro Lett.* **2017**, *6* (2), 68−72.

(11) Mujtaba, A.; Keller, M.; Ilisch, S.; Radusch, H. J.; Beiner, M.; Thurn-Albrecht, T.; Saalwächter, K. Detection of Surface-Immobilized Components and Their Role in Viscoelastic Reinforcement of Rubber−Silica Nanocomposites. *ACS Macro Lett.* **2014**, *3* (5), 481−485.

(12) Cheng, S.; Carroll, B.; Bocharova, V.; Carrillo, J.-M.; Sumpter, B. G.; Sokolov, A. P. Focus: Structure and Dynamics of the Interfacial Layer in Polymer Nanocomposites with Attractive Interactions. *J. Chem. Phys.* **2017**, *146* (20), 203201.

(13) Cheng, S. W.; Holt, A. P.; Wang, H. Q.; Fan, F.; Bocharova, V.; Martin, H.; Etampawala, T.; White, B. T.; Saito, T.; Kang, N. G.; Dadmun, M. D.; Mays, J. W.; Sokolov, A. P., Unexpected Molecular Weight Effect in Polymer Nanocomposites. *Phys. Rev. Lett.* **2016**, *116* (3). DOI: 10.1103/PhysRevLett.116.038302

(14) Holt, A. P.; Bocharova, V.; Cheng, S.; Kisliuk, A. M.; White, B. T.; Saito, T.; Uhrig, D.; Mahalik, J. P.; Kumar, R.; Imel, A. E.; Etampawala, T.; Martin, H.; Sikes, N.; Sumpter, B. G.; Dadmun, M. D.; Sokolov, A. P. Controlling Interfacial Dynamics: Covalent Bonding Versus Physical Adsorption in Polymer Nanocomposites. *ACS Nano* **2016**, *10* (7), 6843−6852.

(15) Jouault, N.; Zhao, D.; Kumar, S. K. Role of Casting Solvent on Nanoparticle Dispersion in Polymer Nanocomposites. *Macromolecules* **2014**, *47* (15), 5246−5255.

DOI: 10.1021/acsami.9b04553
ACS Appl. Mater. Interfaces 2019, 11, 17863−17872

(16) Zhao, D.; Schneider, D.; Fytas, G.; Kumar, S. K. Controlling the Thermomechanical Behavior of Nanoparticle/Polymer Films. *ACS Nano* **2014**, *8* (8), 8163−8173.
(17) Le Strat, D.; Dalmas, F.; Randriamahefa, S.; Jestin, J.; Wintgens, V. Mechanical Reinforcement in Model Elastomer Nanocomposites with Tuned Microstructure and Interactions. *Polymer* **2013**, *54* (5), 1466−1479.
(18) Meth, J. S.; Zane, S. G.; Chi, C.; Londono, J. D.; Wood, B. A.; Cotts, P.; Keating, M.; Guise, W.; Weigand, S. Development of Filler Structure in Colloidal Silica-Polymer Nanocomposites. *Macromolecules* **2011**, *44* (20), 8301−8313.
(19) Zhang, Q.; Archer, L. A. Poly(Ethylene Oxide)/Silica Nanocomposites: Structure and Rheology. *Langmuir* **2002**, *18* (26), 10435−10442.
(20) Chevigny, C.; Dalmas, F.; Di Cola, E.; Gigmes, D.; Bertin, D.; Boué, F.; Jestin, J. Polymer-Grafted Nanoparticles Nanocomposites: Dispersion, Grafted Chain Conformation,and Rheological Behaviour. *Macromolecules* **2011**, *44* (1), 122−133.
(21) Kumar, S. K.; Jouault, N.; Benicewicz, B.; Neely, T. Nanocomposites with Polymer Grafted Nanoparticles. *Macromolecules* **2013**, *46* (9), 3199−3214.
(22) Füllbrandt, M.; Purohit, P. J.; Schönhals, A. Combined FTIR and Dielectric Investigation of Poly(Vinyl Acetate) Adsorbed on Silica Particles. *Macromolecules* **2013**, *46* (11), 4626−4632.
(23) Jia, X. L.; Listak, J.; Witherspoon, V.; Kalu, E. E.; Yang, X. P.; Bockstaller, M. R. Effect of Matrix Molecular Weight on the Coarsening Mechanism of Polymer-Grafted Gold Nanocrystals. *Langmuir* **2010**, *26* (14), 12190−12197.
(24) Janes, D. W.; Moll, J. F.; Harton, S. E.; Durning, C. J. Dispersion Morphology of Poly(Methyl Acrylate)/Silica Nanocomposites. *Macromolecules* **2011**, *44* (12), 4920−4927.
(25) Heo, K.; Miesch, C.; Emrick, T.; Hayward, R. C. Thermally Reversible Aggregation of Gold Nanoparticles in Polymer Nanocomposites through Hydrogen Bonding. *Nano Lett.* **2013**, *13* (11), 5297−5302.
(26) Mackay, M. E.; Tuteja, A.; Duxbury, P. M.; Hawker, C. J.; Van Horn, B.; Guan, Z.; Chen, G.; Krishnan, R. S. General Strategies for Nanoparticle Dispersion. *Science* **2006**, *311* (5768), 1740−1743.
(27) Baeza, G. P.; Genix, A. C.; Degrandcourt, C.; Petitjean, L.; Gummel, J.; Couty, M.; Oberdisse, J. Multiscale Filler Structure in Simplified Industrial Nanocomposite Silica/SBR Systems Studied by SAXS and TEM. *Macromolecules* **2013**, *46* (1), 317−329.
(28) Banc, A.; Genix, A. C.; Chirat, M.; Dupas, C.; Caillol, S.; Sztucki, M.; Oberdisse, J. Tuning Structure and Rheology of Silica-Latex Nanocomposites with the Molecular Weight of Matrix Chains: A Coupled SAXS-TEM-Simulation Approach. *Macromolecules* **2014**, *47* (9), 3219−3230.
(29) Kim, S.; Hyun, K.; Struth, B.; Ahn, K. H.; Clasen, C. Structural Development of Nanoparticle Dispersion During Drying in Polymer Nanocomposite Films. *Macromolecules* **2016**, *49* (23), 9068−9079.
(30) Starr, F. W.; Douglas, J. F.; Meng, D.; Kumar, S. K. Bound Layers "Cloak" Nanoparticles in Strongly Interacting Polymer Nanocomposites. *ACS Nano* **2016**, *10* (12), 10960−10965.
(31) Ciprari, D.; Jacob, K.; Tannenbaum, R. Characterization of Polymer Nanocomposite Interphase and its Impact on Mechanical Properties. *Macromolecules* **2006**, *39* (19), 6565−6573.
(32) Burnside, S. D.; Giannelis, E. P. Nanostructure and Properties of Polysiloxane-Layered Silicate Nanocomposites. *J. Polym. Sci., Part B: Polym. Phys.* **2000**, *38* (12), 1595−1604.
(33) Scheutjens, J. M. H. M.; Fleer, G. J. Statistical Theory of the Adsorption of Interacting Chain Molecules. 2. Train, Loop, and Tail Size Distribution. *J. Phys. Chem.* **1980**, *84* (2), 178−190.
(34) Jouault, N.; Moll, J. F.; Meng, D.; Windsor, K.; Ramcharan, S.; Kearney, C.; Kumar, S. K. Bound Polymer Layer in Nanocomposites. *ACS Macro Lett.* **2013**, *2* (5), 371−374.
(35) Lindner, P.; Zemb, T. *Neutrons, X-Ray and Light Scattering*; North Holland, Elsevier: Amsterdam, 2002.
(36) Papon, A.; Saalwächter, K.; Schäler, K.; Guy, L.; Lequeux, F.; Montes, H. Low-Field NMR Investigations of Nanocomposites: Polymer Dynamics and Network Effects. *Macromolecules* **2011**, *44* (4), 913−922.
(37) Roh, J. H.; Tyagi, M.; Hogan, T. E.; Roland, C. M. Space-Dependent Dynamics in 1,4-Polybutadiene Nanocomposite. *Macromolecules* **2013**, *46* (16), 6667−6669.
(38) Ashkar, R.; Abdul Baki, M.; Tyagi, M.; Faraone, A.; Butler, P.; Krishnamoorti, R. Kinetic Polymer Arrest in Percolated SWNT Networks. *ACS Macro Lett.* **2014**, *3* (12), 1262−1265.
(39) Krutyeva, M.; Wischnewski, A.; Monkenbusch, M.; Willner, L.; Maiz, J.; Mijangos, C.; Arbe, A.; Colmenero, J.; Radulescu, A.; Holderer, O.; Ohl, M.; Richter, D. Effect of Nanoconfinement on Polymer Dynamics: Surface Layers and Interphases. *Phys. Rev. Lett.* **2013**, *110* (10), 108303.
(40) Sargsyan, A.; Tonoyan, A.; Davtyan, S.; Schick, C. The Amount of Immobilized Polymer in Pmma SiO2 Nanocomposites Determined from Calorimetric Data. *Eur. Polym. J.* **2007**, *43*, 3113.
(41) Genix, A.-C.; Bocharova, V.; Kisliuk, A.; Carroll, B.; Zhao, S.; Oberdisse, J.; Sokolov, A. P. Enhancing the Mechanical Properties of Glassy Nanocomposites by Tuning Polymer Molecular Weight. *ACS Appl. Mater. Interfaces* **2018**, *10* (39), 33601−33610.
(42) Cotton, J. P. Variations on Contrast in Sans: Determination of Self and Distinct Correlation Functions. *Adv. Colloid Interface Sci.* **1996**, *69*, 1−29.
(43) Benoit, H. C.; Higgins, J. S. *Polymers and Neutron Scattering*; Oxford University Press: Oxford, 1994.
(44) Genix, A.-C.; Oberdisse, J. Determination of the Local Density of Polydisperse Nanoparticle Assemblies. *Soft Matter* **2017**, *13* (44), 8144−8155.
(45) Cors, M.; Wiehemeier, L.; Hertle, Y.; Feoktystov, A.; Cousin, F.; Hellweg, T.; Oberdisse, J. Determination of Internal Density Profiles of Smart Acrylamide-Based Microgels by SANS: A Multi-Shell Reverse Monte-Carlo Approach. *Langmuir* **2018**, *34* (50), 15403−15415.
(46) Kamiya, H.; Suzuki, H.; Kato, D.; Jimbo, G. Densification of Alkoxide-Derived Fine Silica Powder Compact by Ultra-High-Pressure Cold Isostatic Pressing. *J. Am. Ceram. Soc.* **1993**, *76* (1), 54−64.
(47) Glinka, C. J.; Barker, J. G.; Hammouda, B.; Krueger, S.; Moyer, J. J.; Orts, W. J. The 30 M Small-Angle Neutron Scattering Instruments at the National Institute of Standards and Technology. *J. Appl. Crystallogr.* **1998**, *31* (3), 430−445.
(48) Kline, S. Reduction and Analysis of SANS and USANS Data Using Igor Pro. *J. Appl. Crystallogr.* **2006**, *39* (6), 895−900.

DOI: 10.1021/acsami.9b04553
ACS Appl. Mater. Interfaces 2019, 11, 17863−17872